A HYBRID 3D TLM-FDTD MODEL OF MICROWAVE FIELDS

Channabasappa Eswarappa, *Member, IEEE* and Wolfgang J. R. Hoefer, *Fellow, IEEE*

NSERC/MPR Teltech Research Chair in RF Engineering, Department of Electrical and Computer Engineering, University of Victoria, Victoria, B.C., V8W 3P6, Canada

ABSTRACT

This paper presents a hybrid method which combines 3D Symmetrical Condensed Node -Transmission Line Modeling (SCN-TLM) and Yee's Finite Difference Time Domain (FDTD) methods. This work is an extension of our earlier work on the interface between 2D TLM and FDTD. Even though, the 3D SCN-TLM and FDTD nodes differ in structure and high-frequency dispersion characteristics, they give virtually the same numerical results for identical band-limited excitation, and equal space and time resolution. Using the interface presented in this paper, the specific features of both of these nodes can be exploited when solving a given problem.

INTRODUCTION

Hybrid analysis or combination of different numerical techniques often yields improvements in efficiency and accuracy when solving a given problem. For example, there have been efforts to hybridize FDTD with finite elements in time-domain [1], and mode matching with TLM [2], etc. Among the time-domain numerical methods, TLM and FDTD are very closely related; both are extensively used to analyze electromagnetic structures of arbitrary geometry. The main difference resides in the formulation of the field equations: FDTD algorithms update total field components in a space and time grid, while TLM tracks incident and reflected voltage pulses in a spatial network of transmission lines. Very recently, Celuch-Marcysiak and Gwarek have given the equivalent excitation schemes that produce identical field values at all time steps in the expanded TLM and FDTD meshes [3].

The TLM method has advantages in accurately describing boundaries and dielectric interfaces, while the FDTD method requires less computer memory and time. Also the performance of one-way absorbing boundaries is better when implemented in TLM [4-5]. Hence, hybridizing these two methods will lead to more efficient and accurate algorithms. Recently, we have developed an interface between 2D shunt TLM and 2D FDTD modules, and applied it to implement Berenger's perfectly matched layer (PML) absorbing boundary conditions in TLM [6]. Even though several papers have been published on the relationship between the SCN-TLM and FDTD, no attempt has been made so far to actually link them in a single computer program [7-9]. In this paper, the technique for combining 3D SCN-TLM and FDTD will be reported and validated.

INTERFACE BETWEEN 3D SCN-TLM AND YEE'S FDTD

Yee's FDTD node [10] and Johns' 3D SCN-TLM node [11] are shown in Figs. 1a and 1b, respectively. One major difference between the SCN-TLM and FDTD nodes is that in the SCN-TLM node all six field components are simultaneously available at the centre of the node and at the cell borders at alternate half time steps, while in the FDTD node, E and H components are available at different points and at different half time steps. We have considered a 3D computational space half discretized with a FDTD mesh and half with a SCN-TLM mesh. The interface is parallel to the yz plane (see Fig. 2). For clarity, only one layer of FDTD and SCN-TLM cells is shown. Both subdomains overlap by one cell width Δl; the TLM voltage impulses and the FDTD fields must be linked at the common nodes. Because of the condensed and distributed nature of the fields in the SCN-TLM and FDTD nodes, respectively, the linking is not as straightforward as in the two-dimensional case [6]. The exchange of information between TLM voltage impulses and FDTD field values requires condensing of some FDTD electric field values to the centre of the cells, and expanding of some SCN-TLM electric field values (to the positions corresponding to the FDTD electric field positions).

To implement scattering at the SCN-TLM nodes along the first column of the TLM subpart at (i = I+3/2), we need to inject voltage impulses ${}_{inc}V$ through their free branches from the FDTD subdomain. These impulses can be com-

WE 3F

0-7803-3246-6/96/$5.00 © IEEE

puted by forcing the node voltages to be equal to the condensed electric field values E_{yc} at the centres of the nodes obtained with the FDTD algorithm. For example, the impulses ${}_{inc}V_3$ incident on the nodes can be obtained by subtracting the other three voltage impulses from E_{yc} at these points:

$$
\begin{aligned}
{}_{inc}V_3^{\,n-\frac{1}{2}}(I+\tfrac{3}{2},j+\tfrac{1}{2},k+\tfrac{1}{2}) &= 2E_{yc}^{n}(I+\tfrac{3}{2},j+\tfrac{1}{2},k+\tfrac{1}{2})\times\Delta l \\
&- {}_{inc}\Big[V_4(I+\tfrac{3}{2},j+\tfrac{1}{2},k+\tfrac{1}{2}) + V_8(I+\tfrac{3}{2},j+\tfrac{1}{2},k+\tfrac{1}{2}) \\
&+ V_{11}(I+\tfrac{3}{2},j+\tfrac{1}{2},k+\tfrac{1}{2})\Big]^{n-\frac{1}{2}}
\end{aligned}
\tag{1}
$$

where E_{yc} is calculated by taking the average of the four cell boundary FDTD E_y values:

$$
\begin{aligned}
E_{yc}(I+\tfrac{3}{2},j+\tfrac{1}{2},k+\tfrac{1}{2}) &= \Big[E_y(I+1,j+\tfrac{1}{2},k) + \\
&E_y(I+2,j+\tfrac{1}{2},k) + E_y(I+1,j+\tfrac{1}{2},k+1) + \\
&E_y(I+2,j+\tfrac{1}{2},k+1)\Big]/4
\end{aligned}
\tag{2}
$$

Similarly ${}_{inc}V_6$ can be obtained using the following equations;

$$
\begin{aligned}
{}_{inc}V_6^{\,n-\frac{1}{2}}(I+\tfrac{3}{2},j+\tfrac{1}{2},k+\tfrac{1}{2}) &= 2E_{zc}^{n}(I+\tfrac{3}{2},j+\tfrac{1}{2},k+\tfrac{1}{2})\times\Delta l \\
&- {}_{inc}\Big[V_5(I+\tfrac{3}{2},j+\tfrac{1}{2},k+\tfrac{1}{2}) + V_7(I+\tfrac{3}{2},j+\tfrac{1}{2},k+\tfrac{1}{2}) \\
&+ V_{10}(I+\tfrac{3}{2},j+\tfrac{1}{2},k+\tfrac{1}{2})\Big]^{n-\frac{1}{2}}
\end{aligned}
\tag{3}
$$

$$
\begin{aligned}
E_{zc}(I+\tfrac{3}{2},j+\tfrac{1}{2},k+\tfrac{1}{2}) &= \Big[E_z(I+1,j,k+\tfrac{1}{2}) + \\
&E_z(I+2,j,k+\tfrac{1}{2}) + E_z(I+1,j+1,k+\tfrac{1}{2}) + \\
&E_z(I+2,j+1,k+\tfrac{1}{2})\Big]/4
\end{aligned}
\tag{4}
$$

On the other hand, updating of H_y and H_z of the FDTD nodes in the last column of the FDTD subpart at i = I+2 needs E_y and E_z components at i=I+3:

$$
\begin{aligned}
H_y^{n+\frac{1}{2}}(I+\tfrac{5}{2},j,k+\tfrac{1}{2}) &= H_y^{n-\frac{1}{2}}(I+\tfrac{5}{2},j,k+\tfrac{1}{2}) \\
&+ \frac{\Delta t}{\mu_0\Delta l}\Big[E_{zd}^{n}(I+3,j,k+\tfrac{1}{2}) - E_z^{n}(I+2,j,k+\tfrac{1}{2}) \\
&+ E_x^{n}(I+\tfrac{5}{2},j,k) - E_x^{n}(I+\tfrac{5}{2},j,k+1)\Big]
\end{aligned}
\tag{5}
$$

$$
\begin{aligned}
H_z^{n+\frac{1}{2}}(I+\tfrac{5}{2},j+\tfrac{1}{2},k) &= H_z^{n-\frac{1}{2}}(I+\tfrac{5}{2},j+\tfrac{1}{2},k) \\
&+ \frac{\Delta t}{\mu_0\Delta l}\Big[E_x^{n}(I+\tfrac{5}{2},j+1,k) - E_x^{n}(I+\tfrac{5}{2},j,k) \\
&+ E_y^{n}(I+2,j+\tfrac{1}{2},k) - E_{yd}^{n}(I+3,j+\tfrac{1}{2},k)\Big]
\end{aligned}
\tag{6}
$$

where the cell boundary electric fields E_{yd} and E_{zd} are computed by averaging four electric field values at the neighboring SCN-TLM node centres:

$$
\begin{aligned}
E_{yd}(I+3,j+\tfrac{1}{2},k) &= \Big[E_y(I+\tfrac{7}{2},j+\tfrac{1}{2},k+\tfrac{1}{2}) \\
&+ E_y(I+\tfrac{7}{2},j+\tfrac{1}{2},k-\tfrac{1}{2}) + E_y(I+\tfrac{5}{2},j+\tfrac{1}{2},k+\tfrac{1}{2}) \\
&+ E_y(I+\tfrac{5}{2},j+\tfrac{1}{2},k-\tfrac{1}{2})\Big]/4
\end{aligned}
\tag{7}
$$

$$
\begin{aligned}
E_{zd}(I+3,j,k+\tfrac{1}{2}) &= \Big[E_z(I+\tfrac{7}{2},j+\tfrac{1}{2},k+\tfrac{1}{2}) \\
&+ E_z(I+\tfrac{7}{2},j-\tfrac{1}{2},k+\tfrac{1}{2}) + E_z(I+\tfrac{5}{2},j+\tfrac{1}{2},k+\tfrac{1}{2}) \\
&+ E_z(I+\tfrac{5}{2},j-\tfrac{1}{2},k+\tfrac{1}{2})\Big]/4
\end{aligned}
\tag{8}
$$

The electric field values at the SCN-TLM node centres are, in turn, given by

$$
\begin{aligned}
E_y(i+\tfrac{1}{2},j+\tfrac{1}{2},k+\tfrac{1}{2}) &= \Big[V_3(i+\tfrac{1}{2},j+\tfrac{1}{2},k+\tfrac{1}{2}) \\
&+ V_4(i+\tfrac{1}{2},j+\tfrac{1}{2},k+\tfrac{1}{2}) + V_8(i+\tfrac{1}{2},j+\tfrac{1}{2},k+\tfrac{1}{2}) \\
&+ V_{11}(i+\tfrac{1}{2},j+\tfrac{1}{2},k+\tfrac{1}{2})\Big]/(2\times\Delta l)
\end{aligned}
\tag{9}
$$

$$
\begin{aligned}
E_z(i+\tfrac{1}{2},j+\tfrac{1}{2},k+\tfrac{1}{2}) &= \Big[V_5(i+\tfrac{1}{2},j+\tfrac{1}{2},k+\tfrac{1}{2}) \\
&+ V_6(i+\tfrac{1}{2},j+\tfrac{1}{2},k+\tfrac{1}{2}) + V_7(i+\tfrac{1}{2},j+\tfrac{1}{2},k+\tfrac{1}{2}) \\
&+ V_{10}(i+\tfrac{1}{2},j+\tfrac{1}{2},k+\tfrac{1}{2})\Big]/(2\times\Delta l)
\end{aligned}
\tag{10}
$$

This completes the connection of the two algorithms.

VALIDATION AND NUMERICAL RESULTS

We have tested the above procedure by applying it to a cubic metallic cavity of size 7.112 mm. For a space resolution Δl of 0.16933 mm, the total number of cells is 42x42x42. It was subdivided into a FDTD mesh of size (21x42x42) and a SCN-TLM mesh of size (21x42x42). First, it was impulsively excited in the FDTD subpart with

a TE_{10} mode spatial distribution. The frequency spectrum obtained is plotted in Fig. 3a. It compares well with the frequency spectrum of the cavity discretized exclusively with an FDTD mesh except for a little difference in the higher end of the spectrum (Fig. 3b). This can be attributed to the different dispersion characteristics of the SCN-TLM and FDTD nodes. To ascertain this, the cavity was excited with cosine modulated narrow (containing the frequency components from 20 to 120 GHz) and wide (containing the frequency components from 20 to 35 GHz) Gaussian pulses. The time-domain responses are plotted in Figs. 4a and 4b. We can see that for a wide cosine modulated Gaussian pulse excitation, the response of the hybrid FDTD+TLM mesh is exactly equal to that obtained with an exclusive FDTD mesh. Indeed, both schemes have virtually identical dispersion at the lower end of the spectrum.

CONCLUSIONS

A hybrid SCN-TLM/FDTD numerical algorithm has been successfully developed and validated. Numerical solutions travel seamlessly between the two types of meshes, provided that band-limited excitations are used. This procedure gives us the freedom of choosing the most appropriate discretization approach in different parts of the computational domain. Now, any new development in the FDTD method can be used in the TLM method without deriving its equivalent transmission line network model, or vice versa.

REFERENCES

[1] R. Wu and T. Itoh, "Hybridizing FD-TD Analysis with Unconditionally Stable FEM for Objects of Curved Boundary", in 1995 *IEEE MTTS Digest*, pp. 833-836.

[2] M. Righi and W.J. R. Hoefer, "Efficient 3D-SCN-TLM Diakoptics for Waveguide Components", *IEEE Trans. on MTT*, vol. 42, no. 12, pp. 2381-2385, Dec. 1994.

[3] M. Celuch-Marcysiak and W.K. Gwarek, "Generalized TLM Algorithms with Controlled Stability Margin and Their Equivalence with Finite-Difference Formulations for Modified Grids", *IEEE Trans. Microwave Theory and Techniques*, vol. 43, no. 9, pp. 2081-2089, Sept. 1995.

[4] A. Giannopoulos and J.M. Tealby, "Comparison of Performance of Absorbing Boundary Conditions in TLM and FDTD", *Electronics Letters*, vol. 31, no. 19, pp. 1639-1640, 14th September 1995.

[5] C. Eswarappa and W.J.R. Hoefer, "A Comparative performance study of absorbing boundary conditions in TLM and FDTD", accepted for presentation at the *12th Annual Review of Progress in Applied Computational Electromagnetics* 1996, March 18-22, 1996, Monterey, CA.

[6] C. Eswarappa and W.J.R. Hoefer, "Implementation of Berenger Absorbing Boundary Conditions in TLM by interfacing FDTD Perfectly Matched Layers", *Electronics Letters*, vol. 31, no. 15, pp. 1264-1266, 20th July 1995.

[7] M. Krumpholz and P. Russer, "A Field Theoretical Derivation of TLM", *IEEE Trans. Microwave Theory and Techniques*, vol. 39, no. 3, pp. 1660-1668, Sep. 1994.

[8] H. Jin and R. Vahldieck, "Direct Derivations of TLM Symmetrical Condensed Node and Hybrid Symmetrical Condensed Node from Maxwell's Equations Using Centered Differencing and Averaging", *IEEE Trans. on MTT*, vol. 42, no. 12, pp. 2554-2561, Dec. 1994.

[9] Z. Chen, M.M. Ney, and W.J.R. Hoefer, "A New Finite-Difference Time-Domain Formulation and its Equivalence with the TLM Symmetrical Condensed Node", *IEEE Trans. Microwave Theory and Techniques*, vol. 39, no. 12, pp. 2160-2169, Dec. 1991.

[10] K.S. Yee, "Numerical Solution of Initial Boundary Value Problems Involving Maxwell's Equations", *IEEE Trans. on AP*, vol. 14, no.3, pp. 302-307, May 1966.

[11] P. B. Johns, "Symmetrical Condensed Node for the TLM method", *IEEE Trans. Microwave Theory Tech.*, vol. MTT-35, no. 4, pp. 370-377, April 1987.

ACKNOWLEDGMENTS

This research has been funded by the Natural Sciences and Engineering Research Council of Canada, the Science Council of British Columbia, MPR Teltech Inc. of Burnaby, B.C., and the University of Victoria.

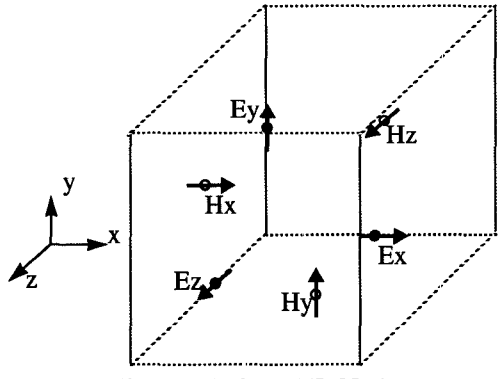

Fig. 1a: Yee's FDTD Node

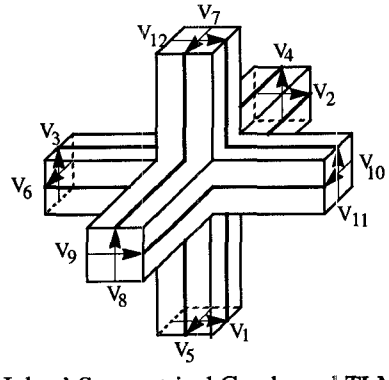

Fig. 1b: Johns' Symmetrical Condensed TLM Node

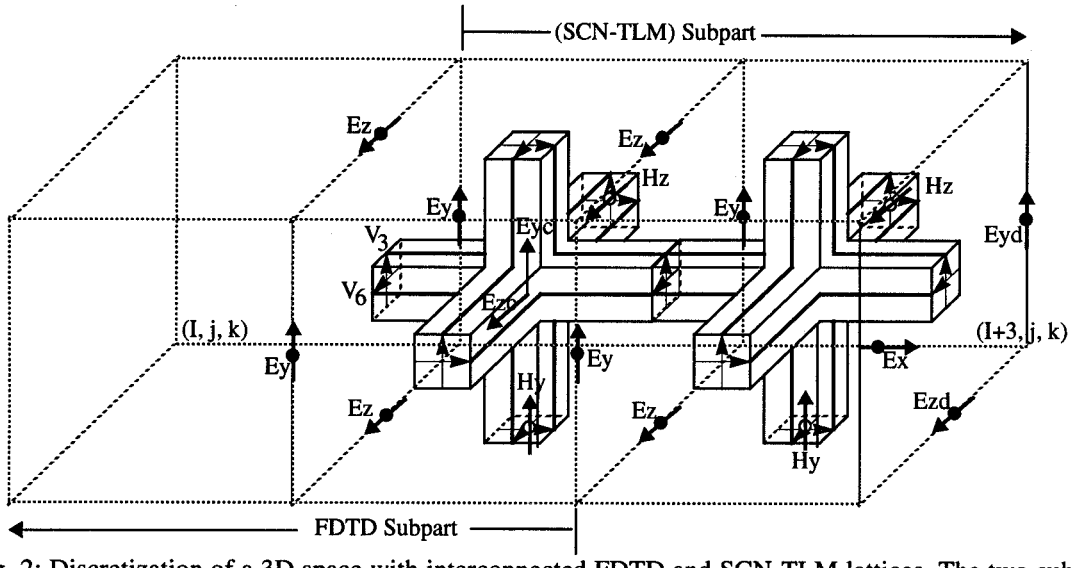

Fig. 2: Discretization of a 3D space with interconnected FDTD and SCN-TLM lattices. The two subdomains overlap by one cell width. The algorithms are coupled by equating two collocated field components in each common cell.

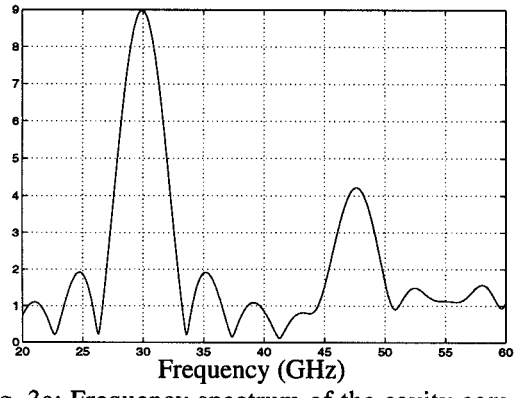

Fig. 3a: Frequency spectrum of the cavity computed with a FDTD+TLM mesh for impulsive excitation.

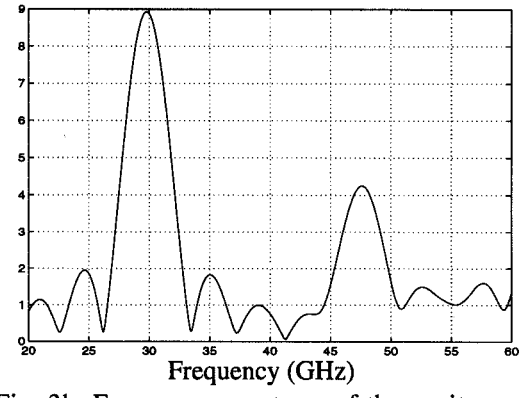

Fig. 3b: Frequency spectrum of the cavity computed with an exclusive FDTD mesh for impulsive excitation.

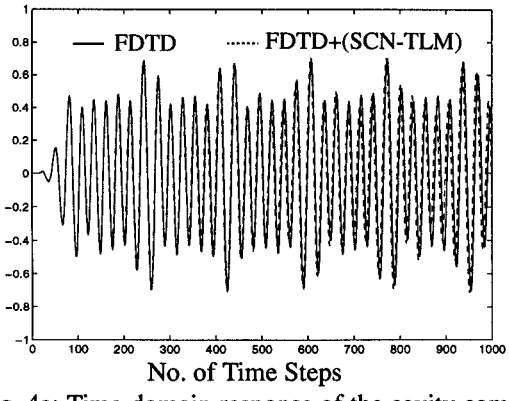

Fig. 4a: Time-domain response of the cavity computed with a FDTD+TLM mesh and an exclusive FDTD mesh for cosine modulated short Gaussian pulse excitation.

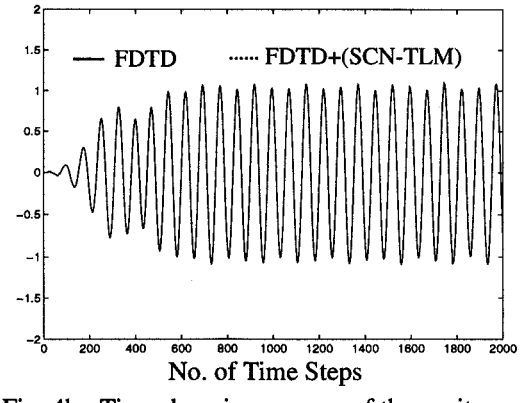

Fig. 4b: Time-domain response of the cavity computed with a FDTD+TLM mesh and an exclusive FDTD mesh for cosine modulated wide Gaussian pulse excitation.